How to cite: *Angew. Chem. Int. Ed.* **2021**, *60*, 2393–2397
International Edition: doi.org/10.1002/anie.202011544
German Edition: doi.org/10.1002/ange.202011544

Imaging

A General Strategy to Design Highly Fluorogenic Far-Red and Near-Infrared Tetrazine Bioorthogonal Probes

*Wuyu Mao, Jie Tang, Liqun Dai, Xinyu He, Jie Li, Larry Cai, Ping Liao, Ruotian Jiang, Jingwei Zhou, and Haoxing Wu**

Abstract: *Highly fluorogenic tetrazine bioorthogonal probes emitting at near-infrared wavelengths are in strong demand for biomedical imaging applications. Herein, we have developed a strategy for forming a palette of novel Huaxi-Fluor probes in situ, whose fluorescence increases hundreds of times upon forming the bioorthogonal reaction product, pyridazine. The resulting probes show large Stokes shifts and high quantum yields. Manipulating the conjugate length and pull–push strength in the fluorophore skeleton allows the emission wavelength to be fine-tuned from 556 to 728 nm. The highly photo-stable and biocompatible probes are suitable for visualizing organelles in live cells without a washing step and for imaging of tumors in live small animals to depths of 500 μm by two-photon excitation.*

Introduction

With its recent debut in a clinical trial, tetrazine bioorthogonal chemistry is progressing from cutting-edge laboratory technology to next generation theranostic tool.[1] It is being used to activate drugs in a specific manner,[2] non-invasively image immune responses[3] and guide the design of antibody-drug conjugates.[4] Tetrazine-based fluorogenic probes have been developed to visualize specific biomolecules with high spatio-temporal resolution in live cells,[5] which may make them capable of delineating key structures during image-guided surgery.[6]

[*] Dr. W. Mao, L. Dai, X. He, J. Li, Prof. H. Wu
Huaxi MR Research Center, Department of Nuclear Medicine, Frontiers Science Center for Disease-related Molecular Network, National Clinical Research Center for Geriatrics
West China Hospital, Sichuan University
Chengdu 610041 (China)
E-mail: haoxingwu@scu.edu.cn

Dr. J. Tang, L. Cai
Australian Institute for Bioengineering and Nanotechnology
The University of Queensland
St Lucia, Brisbane, QLD 4072 (Australia)

P. Liao, Prof. R. Jiang
Laboratory of Anesthesia and Critical Care Medicine, Department of Anesthesiology, West China Hospital of Sichuan University
Chengdu, Sichuan 610000 (China)

Dr. J. Zhou
Institute of clinical pharmacology, Science and Technology Innovation Center, Guangzhou University of Chinese Medicine
Guangzhou 510405, Guangdong (China)

Supporting information and the ORCID identification number(s) for the author(s) of this article can be found under: https://doi.org/10.1002/anie.202011544.

The rationale behind using tetrazine bioorthogonal chemistry to generate fluorogenic probes is that the probe is prepared as a non- or weakly fluorescent precursor that undergoes a bioorthogonal reaction to become strongly fluorescent. Upon reaction, the fluorescence of the probes should increase more than 100-fold to maximize the signal-to-noise contrast.[7] For the same reason, probes preferably emit strongly in the far-red or near-infrared region with a large Stokes shift, which allows their signal to be differentiated from tissue autofluorescence and with deeper penetration.[8]

Several designs have been used to incorporate tetrazine into fluorogenic probes,[5a,9] beginning with the use of a simple flexible aliphatic linkage by Devaraj et al. to make tetrazine turn-on probes.[10] The Weissleder group used Lewis acid promoted de novo tetrazine synthesis[11] to install tetrazine directly onto skeletons of coumarin or BODIPY.[12] This placed the two chromophores quite close together, dramatically increasing the quench efficiency, such that fluorescence increased up to a thousand-fold upon bioorthogonal activation. The Park group used strong electronic coupling to construct Seoul-Fluor–tetrazine conjugates that emitted wavelengths as long as 580 nm with 600-fold turn-on.[13] To expand the range of skeletons into which it can be integrated, tetrazine can also be converted into π-conjugated derivatives by cross-coupling reactions[5a] suitable for energy transfer and quenching. Even after extensive studies with classical fluorescence cassette, including xanthene, silicon–rhodamine, phenoxazine and cyanine,[5b,12b,14] relatively few highly fluorogenic probes are available that emit in far-red or near-infrared region.

Therefore, the present study aimed to generate tetrazine-based probes whose emission wavelengths could be tuned from the far-red to near-infrared range through altering intramolecular charge-transfer (ICT) processes in the photo-excited state by bioorthogonal reactions.[15] Most tetrazine bioorthogonal reactions yield pyridazine as the product, either directly or after rapid oxidation.[5a,16] Pyridazine is a typical electron-deficient aza-heterocycle[17] while tetrazine is the electron-poorest aromatic system[18] featuring a low lying π* lowest unoccupied molecular orbital (LUMO).[19] We reasoned that if we conjugated an electron donor to tetrazine using a suitable conjugated system, the pyridazine generated in the bioorthogonal reaction could act as electron acceptor to produce in situ a new donor (D)–π-acceptor (A) fluorochrome (Scheme 1). The competing n–π* transition in tetrazine at the lowest excited singlet state should not lead to fluorescence emission.[15,18] Furthermore, we envisioned that by altering the π-conjugation level and electronic

Scheme 1. The strategy for fluorophore in situ formation by tetrazine bioorthogonal reaction.

properties of D-A, we could fine-tune the fluorescence emission from these novel dipolar architectures.

Results and Discussion

We first constructed the cyanine-like probe **1** containing a polymethine conjugated system, using our recently reported Horner–Wadsworth–Emmons reaction for tetrazine derivatization (Table 1).[20] In this probe, the *para*-dimethylaniline acts as the donor, while the hydroxyl group at the 3-position of tetrazine improves solubility with neutral charge. Probe **1**, which emits no detectable fluorescence, reacted nearly quantitatively with bicyclooctyne (BCN) **6** (Supporting Information, Figure S1). The reaction product showed a hypsochromic shift of the absorption peak with a high extinction coefficient of $5.0\times10^4\ M^{-1}cm^{-1}$, indicating the occurrence of ICT.[8] The resulting pyridazine altered charge transfer (CT) in situ, leading the probe to emit bright red fluorescence (λ_{max} 619 nm) that was 1273-fold higher than that from the tetrazine precursor. The new D-A fluorochrome presented a large Stokes shift (212 nm) and moderate quantum yield (6%), and its brightness of $3.0\times10^3\ M^{-1}cm^{-1}$ is comparable to that of some commercial dyes.[21]

Since polymethine can be unstable in vivo, especially in the presence of reactive oxygen species,[22] we investigated the photophysical effects of replacing it with common aromatic rings in the conjugated system (Table 1). Replacement with pyridyl ring caused notable hypochromatic shifts of the absorption and emission bands. Conversely, replacement with electron-rich heteroaromatic furan or thiophene caused bathochromic shifts of the emission band to 622 or 642 nm, respectively. The thiophene-bridged probe **5** showed high quantum yield (30%) and a 961-fold fluorescence increase after bioorthogonal reaction. These results may be due to the ability of the electron-rich heterocyclic bridge to act as an auxiliary donor and the low delocalization energy of thiophene, which further delocalizes π electrons and thereby strengthens conjugation in D-A compounds.[23] Thiophene, for its part, has also been shown to improve photostability and the two-photon absorption (TPA) cross section.[24] We denominated these conjugates of electron donor and tetrazine, connected via a thiophene-containing bridge, as Huaxi-Fluors (**HFs**) followed by their emission maximum, for example, $\mathbf{HF_{642}}$.

Next, we explored whether we could tune the emission wavelength of **HFs** across the far-red and near-infrared range by modifying the length of the conjugated system. This length alters CT energy, which in turn shifts the emission wavelength.[25] When we shortened the conjugation by replacing the styrylthiophene group of $\mathbf{HF_{642}}$ with phenylthiophene, the emission peak shifted to 587 nm in the orange region ($\mathbf{HF_{587}}$, Scheme 2). Replacing the styrylthiophene group with benzothiophene shifted the peak to 556 nm in the green-yellow region ($\mathbf{HF_{556}}$, Scheme 2). Conversely, extending the conjugation in $\mathbf{HF_{642}}$ by replacing the aniline with naphthalenamine caused an 8-nm bathochromic shift in emission ($\mathbf{HF_{650}}$).

We reasoned that we might be able to further tune the emission of **HFs** by altering the electron donating-withdrawing strength of the conjugation system. Indeed, when we replaced the rotatable dimethyl group with a rigid julolidine ring, we pushed emission to 688 nm (Scheme 2). When we increased the electron pull exerted of the pyridazine by replacing the methyl group of $\mathbf{HF_{642}}$ with hydrogen or pyridyl, we observed respective bathochromic shifts of 10 nm ($\mathbf{HF_{652}}$) or 43 nm ($\mathbf{HF_{685}}$).

Table 1: Construction of conjugated systems with various π linkages and photophysical properties of the corresponding fluorophores formed by reaction with **6**.[a]

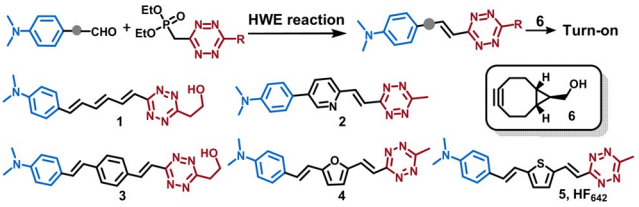

Probe	λ_{ex} [nm]	λ_{em} [nm]	ε[b] $\times10^4$	Turn-on	$\Delta\lambda$[c] [nm]	Φ[d]	$\varepsilon\Phi$[e] $\times10^3$
1	407	619	5.0	1273	212	0.06	3.0
2	378	597	2.5	1100	219	0.12	3.0
3	395	620	3.0	211	225	0.06	1.8
4	423	622	3.4	277	199	0.18	6.1
5/HF_{642}	433	642	3.6	961	209	0.30	10.8

[a] All results were obtained after complete reaction between probes and **6** in EtOH. [b] $L\,mol^{-1}cm^{-1}$. [c] Stokes shift. [d] Quantum yield. [e] Brightness.

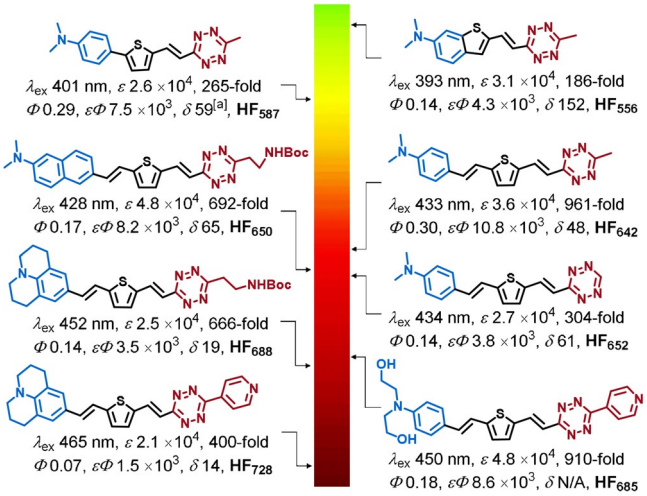

Scheme 2. Chemical structures of Huaxi-Fluors and fine-tuning of their photophysical properties. All results were obtained after complete reaction between probes and **6** in EtOH. [a] TPA cross-section, $10^{-50}\ cm^4\,s\,photon^{-1}$, GM units.

Either adding a julolidine group to $\mathbf{HF}_{642}$ to immobilize the amino group or replacing the methyl in $\mathbf{HF}_{642}$ with a pyridyl group red-shifted probe emission by 43–46 nm. We hypothesized that making these changes at both ends of the probe could shift emission about 85 nm into the near-infrared region. Indeed, both modifications to $\mathbf{HF}_{642}$ led to a probe that, after bioorthogonal reaction emitted at 728 nm ($\mathbf{HF}_{728}$, Scheme 2), which is congruous with our prediction.

Photophysical assessment of all **HFs** showed them to have broad, intense absorption centered around 450 nm, which reflected ICT processes. They showed large Stokes shifts of up to 263 nm, suggesting potential for multicolor imaging (Scheme 2; Supporting Information, Figures S12–S19). All probes showed turn-on ratio of a few hundred folds after bioorthogonal reactions with BCN, which is much higher than the most of previous far-red and near-infrared tetrazine fluorogenic probes.[5a] Quantum yield is in the range of 7–30%, and brightness is on the order of magnitude of 10^4, which should allow imaging without the need to wash out excess probes.[12b] Interestingly, after reacting with *trans*-cyclooctene, the dihydropyridazine adducts produced a similar turn-on ratio but a hypsochromic shift of fluorescence maxima (Supporting Information, Figure S20). Further study on this phenomenon may provide insights for ratiometric probe design, especially for imaging reactive oxidative species. Several probes exhibited TPA cross-sections above 60 GM (Scheme 2; Supporting Information, Figures S12–S19). This suggests potential applications for intravital multiphoton imaging.[26]

To understand the turn-on mechanism, we performed time-dependent density functional theory calculations at the CAM-B3LYP/6-31 + G (d,p) level using the Gaussian 09 package.[27] The geometry optimization calculations of the ground state (S_0) and the excited state (S_1 and S_2) were performed in the polarizable continuum model (Ethanol).[28] And the vibration frequency calculations were also carried out to make sure that the optimized structures were true energy minima. We compared the ICT behavior of probes and the corresponding turn-on products based on molecular orbital features and changes in electron density and dipole moment changes. In general, the computations were consistent with our experimental observations and were able to explain fluorogenesis (Figure 1; Supporting Information, Figures S29–S31). The difference in electron density before and after excitation confirmed local excitation without obvious CT (D index = 0.037 Å) with negligible change of dipolar moment and nearly null oscillator strength for the electronic transition of emission ($f = 0.0078$), confirming the fluorescence quenching mechanism. In contrast, the bioorthogonal product of $\mathbf{HF}_{642}$, called $\mathbf{Pz}_{642}$, showed no tetrazine n–π* transition, and the LUMO-HOMO transition dominated S_1-S_0 excitation. The excitation of $\mathbf{Pz}_{642}$ involved obvious charge transfer and change in dipolar moment (D index = 1.667 Å). Changes in donor charge (0.02143 e) and acceptor charge (−0.01270 e) confirmed the CT excitation. The high oscillator strength for the electronic transition of emission ($f = 1.8036$) confirmed the feasibility of fluorescence emission (Figure 1). In fact, the predicted emission maximum wavelength (622.46 nm) was quite close to the observed one (642 nm).

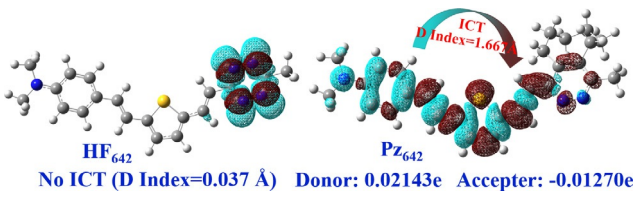

Figure 1. Changes in electron density upon electronic excitation of $\mathbf{HF}_{642}$ and $\mathbf{Pz}_{642}$. Blue and brown denote areas where the electron density decreases and increases. The charge transfer D index or changes in charge are indicated below the structures.

To confirm that **HFs** could undergo rapid bioorthogonal reactions needed for biomedical applications, we measured the kinetics of reaction between **6** and several **HFs** (Supporting Information, Figures S21–S24). The reaction kinetics of **HFs** were similar to those of previous reports.[29] $\mathbf{HF}_{586}$ and $\mathbf{HF}_{645}$ generated turn-on products that were consistently fluorogenic over a pH range from 4.0 to 10.0 (Supporting Information, Figure S25). Moreover, both probes remained stable for hours in cell culture medium with no increase in fluorescence prior to bioorthogonal reaction, and the turn-on by BCN was similarly high immediately or after 3 hours incubation (Supporting Information, Figure S26).

$\mathbf{HF}_{645}$ and $\mathbf{HF}_{586}$ showed negligible toxicity against Hela cells and mesenchymal stem cells: viability was > 97% after incubation for 24 h, based on a standard CCK-8 assay (Supporting Information, Figures S27, S28). When $\mathbf{HF}_{645}$ was administered to SKOV3 cells that had been pre-targeted with BCN conjugated to the epidermal growth factor receptor (EGFR) inhibitor cetuximab, fluorescence activation peaked after 40 min (Figure 2b; Supporting Information, Figure S32). Emission scan of the resulting cetuximab by confocal microscopy illustrated similar fluorescence spectrum with a slightly hypsochromic shift, whereas there is inappreciable signal for the control cetuximab without BCN decorating (Supporting Information, Figure S34). We were happy to find the turn-on ratio is 36-fold without washing steps (Supporting Information, Figure S34). Addition of $\mathbf{HF}_{645}$ to MC3T3 cells that had been pretreated with BCN-morpholine **7** allowed imaging of lysosomes with high signal-to-background contrast without washing out excess probe, while the control group without BCN showed negligible background (Figure 2c–h; Supporting Information, Figure S35). Similar results were observed using a conjugate of BCN-triphenylphosphonium **8** to target mitochondria. The observed signal for lysosomes colocalized with LysoSensor DND189 dye (Pearson's correlation coefficient 0.95 ± 0.04), while the signal for mitochondria colocalized with Mito-tracker dye (0.94 ± 0.03) (Figure 2o–p). Under these conditions, $\mathbf{HF}_{645}$ accumulated in lysosomes: pixel intensity was 14–111 fold higher within the organelles than in areas outside, despite the lack of wash-out (Supporting Information, Figure S35).

We examined the resistance of $\mathbf{HF}_{645}$ to photobleaching, because probes must retain strong signal even with prolonged, repeated laser exposure in order to support high-quality super-resolution imaging and three-dimensional reconstruction. After 100 cycles of irradiation at 488 nm, Mito-Tracker

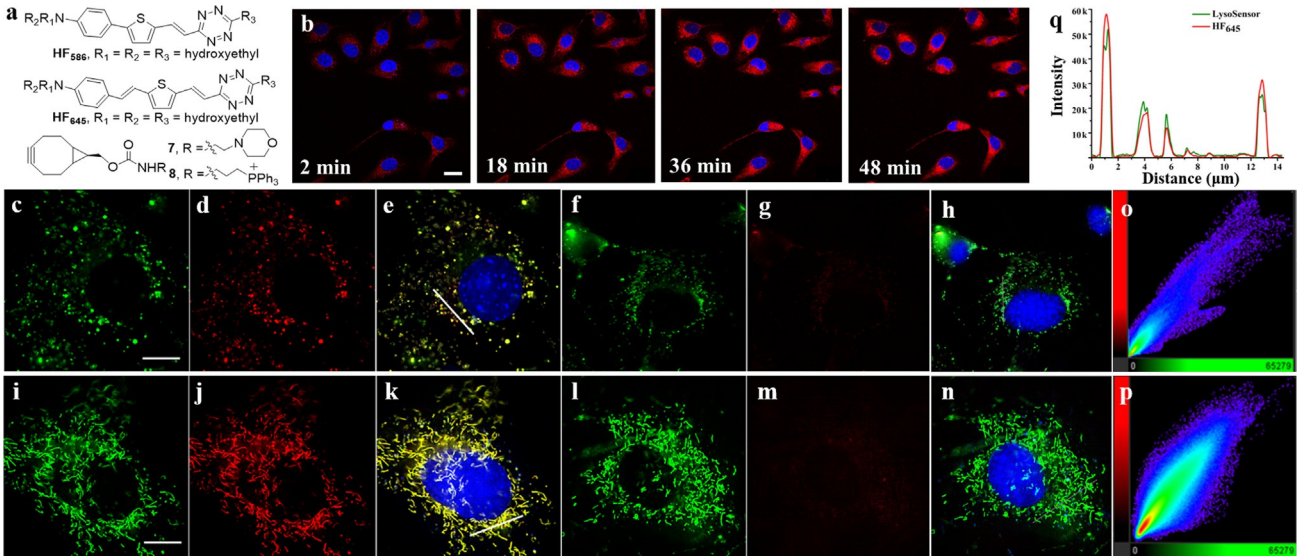

Figure 2. No-wash live-cell imaging of $\mathbf{HF}_{645}$. a) Chemical structures of $\mathbf{HF}_{586}$, $\mathbf{HF}_{645}$, **7** and **8**. b) Time course imaging of EGFR expression on SKOV3 cells. Cells were incubated with BCN-cetuximab (10 nM), washed briefly then imaged immediately after addition of 4 μM $\mathbf{HF}_{645}$. Scale bar, 20 μm. c)–n) Colocalization of $\mathbf{HF}_{645}$ with lysosomes and mitochondrial: MC3T3 cells were incubated with Hoechst dye (c–n) as well as LysoSensor DND189 (c–h), Mito Tracker Green (i–n), **7** (c–e) or **8** (i–k), or DMSO (f–h, l–n). Cells were washed, $\mathbf{HF}_{645}$ was added, and cells were imaged 40 min later without any washes. Scale bar, 10 μm. o) Plot of the fluorescence correlation between LysoSensor dye and $\mathbf{HF}_{645}$ in (e). p) Plot of the fluorescence correlation between Mito Tracker dye and $\mathbf{HF}_{645}$ in image k. q) Plot of pixel fluorescence along the white line in (e). For $\mathbf{HF}_{645}$, ex 488 nm, em 590–650 nm.

Green dye emitted fluorescence at only 22.7 % of the initial intensity, LysoSensor, at only 37.5 %, but $\mathbf{HF}_{645}$, at 57.3 % in the case of mitochondrion and 69.4 % in the case of lysosome (Supporting Information, Figures S36, S37).

Near-infrared fluorescence imaging has played a crucial role in improving surgical cancer outcomes. We investigated the feasibility of our fluorogenic reaction for in vivo imaging, which could potentially avoid long time biodistribution and degrading of probe versus an ex situ labeled antibody-fluor conjugate.[5a] We directly examined the potential of $\mathbf{HF}_{645}$ for in vivo imaging. Mice bearing SKOV3 xenograft tumors overexpressing EGFR were systemically injected first with BCN-cetuximab, then with $\mathbf{HF}_{645}$. Fluorescence of $\mathbf{HF}_{645}$ in tumors was significantly higher in animals treated with the bioorthogonal conjugate than with cetuximab on its own (Figure 3). Conspicuous fluorescence was observed in SKOV3 tumors after 60 min. At 90 min after injection, tumor and various tissues were harvested from animals and $\mathbf{HF}_{645}$ signal was semi-quantified. Signal was 9-fold higher in animals treated with the bioorthogonal conjugate than in animals treated with cetuximab on its own (Supporting Information, Figure S38). Fluorescence signal above background as deep as 500 μm below the surface was detected by Two-photon imaging on tumors in vivo (Supporting Information, Figure S39). These pilot studies suggest that the **HFs** have potential for in vivo imaging with deep penetration.

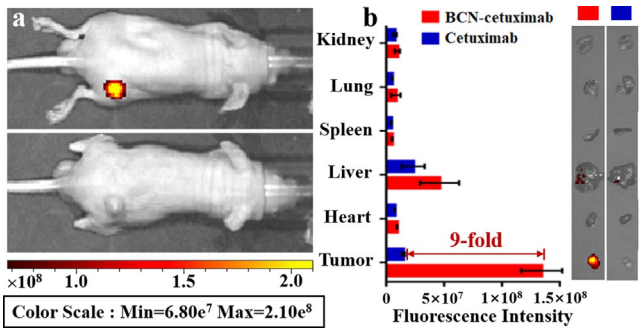

Figure 3. Imaging of $\mathbf{HF}_{645}$ fluorescence in mice in vivo and major organs ex vivo. a) Mice with tumor xenografts were systemically injected first with BCN-cetuximab (top) or cetuximab (bottom), then with $\mathbf{HF}_{645}$ at 60 min later. b) Fluorescence imaging of major organs ex vivo. Ex. 500 ± 15 nm, Em. 600 ± 10 nm.

Conclusion

Here we have described the novel fluorogenic HuaxiFluor probes in which the tetrazine moiety acts not only as a bioorthogonal partner and quencher but also as the core of fluorophore precursor. The reaction product, pyridazine, serves as the electron acceptor, to trigger efficient ICT via a thiophene containing π-bridge. In this way, fluorophore with extremely large Stokes shift and high quantum yield is generated in situ. Altering the length of the conjugate and the ability of the skeleton to pull or push electrons allows fine-tuning of the emission maximum between 556 nm and near-infrared wavelengths. The hundreds-fold gain in fluorescence upon bioorthogonal reaction allows the probes to label subcellular structures in living cells with strong contrast without a washing step. Their TPA and stability in vivo under continuous irradiation suggests that the probes can be used to visualize targets in a wide range of applications. Our approach extends the usefulness of tetrazine-based fluorogenic probes beyond 700 nm, which may pave the way to new biomedical

applications and provide insights into further design of tetrazine-based probes.

Acknowledgements

We acknowledge financial support from National Natural Science Foundation of China (Grant No. 21977075, 21807075). "The Fundamental Research Funds for the Central Universities". China Postdoctoral Science Foundation (2018M643464). "1.3.5 project for disciplines of excellence, West China Hospital, Sichuan University". We would like to thank the Analytical & Testing Center of Sichuan University for NMR Tests.

Conflict of interest

The authors declare no conflict of interest.

Keywords: bioorthogonal chemistry · fluorophores · imaging · near-infrared probes · tetrazine

[1] a) N. K. Devaraj, *ACS Cent. Sci.* **2018**, *4*, 952 – 959; b) M. Peplow, *Nat. Biotechnol.* **2019**, *37*, 835 – 837; c) S. S. Nguyen, A. J. Prescher, *Nat. Rev. Chem.* **2020**, *4*, 476 – 489.

[2] a) A. van Onzen, R. M. Versteegen, F. J. M. Hoeben, I. A. W. Filot, R. Rossin, T. Zhu, J. Wu, P. J. Hudson, H. M. Janssen, W. Ten Hoeve, M. S. Robillard, *J. Am. Chem. Soc.* **2020**, *142*, 10955 – 10963; b) J. M. Mejia Oneto, I. Khan, L. Seebald, M. Royzen, *ACS Cent. Sci.* **2016**, *2*, 476 – 482.

[3] M. Rashidian, E. J. Keliher, A. M. Bilate, J. N. Duarte, G. R. Wojtkiewicz, J. T. Jacobsen, J. Cragnolini, L. K. Swee, G. D. Victora, R. Weissleder, H. L. Ploegh, *Proc. Natl. Acad. Sci. USA* **2015**, *112*, 6146 – 6151.

[4] A. N. Marquard, J. C. T. Carlson, R. Weissleder, *Bioconjugate Chem.* **2020**, *31*, 1616 – 1623.

[5] a) B. L. Oliveira, Z. Guo, G. J. L. Bernardes, *Chem. Soc. Rev.* **2017**, *46*, 4895 – 4950; b) P. Werther, K. Yserentant, F. Braun, N. Kaltwasser, C. Popp, M. Baalmann, D. P. Herten, R. Wombacher, *Angew. Chem. Int. Ed.* **2020**, *59*, 804 – 810; *Angew. Chem.* **2020**, *132*, 814 – 820; c) G. Beliu, A. J. Kurz, A. C. Kuhlemann, L. Behringer-Pliess, M. Meub, N. Wolf, J. Seibel, Z. D. Shi, M. Schnermann, J. B. Grimm, L. D. Lavis, S. Doose, M. Sauer, *Commun. Biol.* **2019**, *2*, 261 – 273.

[6] a) M. Gao, F. B. Yu, C. J. Lv, J. Choo, L. X. Chen, *Chem. Soc. Rev.* **2017**, *46*, 2237 – 2271; b) A. L. Vahrmeijer, M. Hutteman, J. R. van der Vorst, C. J. van de Velde, J. V. Frangioni, *Nat. Rev. Clin. Oncol.* **2013**, *10*, 507 – 518.

[7] B. Huang, H. Babcock, X. W. Zhuang, *Cell* **2010**, *143*, 1047 – 1058.

[8] P. Shieh, C. R. Bertozzi, *Org. Biomol. Chem.* **2014**, *12*, 9307 – 9320.

[9] H. Wu, N. K. Devaraj, *Acc. Chem. Res.* **2018**, *51*, 1249 – 1259.

[10] N. K. Devaraj, S. Hilderbrand, R. Upadhyay, R. Mazitschek, R. Weissleder, *Angew. Chem. Int. Ed.* **2010**, *49*, 2869 – 2872; *Angew. Chem.* **2010**, *122*, 2931 – 2934.

[11] J. Yang, M. R. Karver, W. Li, S. Sahu, N. K. Devaraj, *Angew. Chem. Int. Ed.* **2012**, *51*, 5222 – 5225; *Angew. Chem.* **2012**, *124*, 5312 – 5315.

[12] a) K. S. Yang, G. Budin, C. Tassa, O. Kister, R. Weissleder, *Angew. Chem. Int. Ed.* **2013**, *52*, 10593 – 10597; *Angew. Chem.* **2013**, *125*, 10787 – 10791; b) L. G. Meimetis, J. C. T. Carlson, R. J. Giedt, R. H. Kohler, R. Weissleder, *Angew. Chem. Int. Ed.* **2014**, *53*, 7531 – 7534; *Angew. Chem.* **2014**, *126*, 7661 – 7664.

[13] Y. Lee, W. Cho, J. Sung, E. Kim, S. B. Park, *J. Am. Chem. Soc.* **2018**, *140*, 974 – 983.

[14] a) G. Knorr, E. Kozma, A. Herner, E. A. Lemke, P. Kele, *Chem. Eur. J.* **2016**, *22*, 8972 – 8979; b) A. Wieczorek, P. Werther, J. Euchner, R. Wombacher, *Chem. Sci.* **2017**, *8*, 1506 – 1510; c) H. Wu, J. Yang, J. Seckute, N. K. Devaraj, *Angew. Chem. Int. Ed.* **2014**, *53*, 5805 – 5809; *Angew. Chem.* **2014**, *126*, 5915 – 5919.

[15] A. P. de Silva, H. Q. Gunaratne, T. Gunnlaugsson, A. J. Huxley, C. P. McCoy, J. T. Rademacher, T. E. Rice, *Chem. Rev.* **1997**, *97*, 1515 – 1566.

[16] H. L. Li, Z. Sun, W. T. Wu, X. Wang, M. Q. Zhang, X. J. Lu, W. G. Zhong, D. C. Dai, *Org. Lett.* **2018**, *20*, 7186 – 7191.

[17] B. J. Tabner, J. R. Yandle, *J. Chem. Soc.* **1968**, 381 – 388.

[18] G. Clavier, P. Audebert, *Chem. Rev.* **2010**, *110*, 3299 – 3314.

[19] Q. Zhou, P. Audebert, G. Clavier, R. Meallet-Renault, F. Miomandre, Z. Shaukat, T. T. Vu, J. Tang, *J. Phys. Chem. C* **2011**, *115*, 21899 – 21906.

[20] W. Mao, W. Shi, J. Li, D. Su, X. Wang, L. Zhang, L. Pan, X. Wu, H. Wu, *Angew. Chem. Int. Ed.* **2019**, *58*, 1106 – 1109; *Angew. Chem.* **2019**, *131*, 1118 – 1121.

[21] L. D. Lavis, R. T. Raines, *ACS Chem. Biol.* **2008**, *3*, 142 – 155.

[22] D. Oushiki, H. Kojima, T. Terai, M. Arita, K. Hanaoka, Y. Urano, T. Nagano, *J. Am. Chem. Soc.* **2010**, *132*, 2795 – 2801.

[23] a) P. V. Bedworth, Y. M. Cai, A. Jen, S. R. Marder, *J. Org. Chem.* **1996**, *61*, 2242 – 2246; b) I. D. L. Albert, T. J. Marks, M. A. Ratner, *J. Am. Chem. Soc.* **1997**, *119*, 6575 – 6582; c) J. Roncali, *Chem. Rev.* **1997**, *97*, 173 – 205.

[24] a) S. Maity, S. Das, C. M. Sadlowski, J. T. Zhang, G. K. Vegesna, N. Murthy, *Chem. Commun.* **2017**, *53*, 10184 – 10187; b) H. P. Zhou, F. X. Zhou, S. Y. Tang, P. Wu, Y. X. Chen, Y. L. Tu, J. Y. Wu, Y. P. Tian, *Dyes Pigm.* **2012**, *92*, 633 – 641.

[25] H. Meier, *Angew. Chem. Int. Ed.* **2005**, *44*, 2482 – 2506; *Angew. Chem.* **2005**, *117*, 2536 – 2561.

[26] M. A. Miller, R. Weissleder, *Nat. Rev. Cancer* **2017**, *17*, 399 – 414.

[27] C. Adamo, D. Jacquemin, *Chem. Soc. Rev.* **2013**, *42*, 845 – 856.

[28] E. Cancès, B. Mennucci, J. Tomasi, *J. Chem. Phys.* **1997**, *107*, 3032 – 3041.

[29] X. Li, Z. K. Liu, S. L. Dong, *RSC Adv.* **2017**, *7*, 44470 – 44473.

Manuscript received: August 23, 2020
Revised manuscript received: October 5, 2020
Accepted manuscript online: October 20, 2020
Version of record online: December 1, 2020

